IEEE Access
Multidisciplinary ⋮ Rapid Review ⋮ Open Access Journal

Received April 28, 2021, accepted May 23, 2021, date of publication May 26, 2021, date of current version June 4, 2021.

Digital Object Identifier 10.1109/ACCESS.2021.3083986

A Flexible Vibration Probe Based on PZT Low-Frequency Drive Mode

WEIKANG ZHENG[1], KAI TIAN[1], JUNKANG GUO[1,2], (Member, IEEE), ZHIGANG LIU[1], (Member, IEEE), AND JUN HONG[1], (Member, IEEE)

[1]Key Laboratory of Education Ministry for Modern Design and Rotor-Bearing System, School of Mechanical Engineering, Xi'an Jiaotong University, Xi'an 710049, China
[2]State Key Laboratory of Smart Manufacturing for Special Vehicles and Transmission System, Baotou 014030, China

Corresponding author: Zhigang Liu (mezgliu@mail.xjtu.edu.cn)

This work was supported in part by the Natural Science Foundation of China under Grant 51875447 and Grant 51805419, and in part by the Foundation of State Key Laboratory of Smart Manufacturing for Special Vehicles and Transmission System under Grant GZ2019KF005.

ABSTRACT Precision contact probes have a huge demand in industrial manufacturing due to their high accuracy. However, the passive measurement mode of the existing probe easily causes wear of the probe ball and loss of accuracy during continuous contact scanning. In this paper, a PZT(piezoelectric actuators)-driven flexible probe is proposed with the dynamic time-domain function of the system response from low frequency to high drive frequency. The low-frequency measurement mode is established based on the linear response of the triangle wave. In order to avoid the trajectory nonlinearity of the stylus ball driven by PZT, the nonlinear mapping of the PZT hysteresis model is constructed by the BP neural network, and the linearly weighted particle swarm optimization (PSO) algorithm is used to realize the suppression of the response nonlinearity. Finally, the measurement experiment of the PZT-driven probe is conducted to reveal the measurement characteristics of low-frequency mode as well as measurement capability compared with commercial sensors.

INDEX TERMS PZT-driven probe, low-frequency mode, trajectory nonlinearity, nonlinear suppression.

I. INTRODUCTION

Precision probes have a wide range of applications in industrial manufacturing measurement. Especially in the current research and development of intelligent manufacturing [1], micro/nano probes are playing an increasingly important role in providing high-quality data for industrial digital twins [2], [3]. However, for industrial-grade contact precision probes, the passive measurement mode of force stimulation-deformation-electrical signal response [4], [5] is becoming a factor restricting accuracy. Specifically, the collision and wear of the stylus ball of the probe [6], [7] and the inevitable scanning friction during continuous scanning are leading to the accuracy degradation of measurement result [8], [9].

For contact measurement, the high flexibility of the probe itself [10] is not only the main method to reduce the wear of the probe during the scanning process, but also can weaken the time-varying friction caused by the normal movement of the probe. Fundamentally speaking, friction is the direct cause of ball wear. Li *et al.* [11], Liebrich and Knapp [12] and He *et al.* [13] have greatly improved the flexibility of the probe by cleverly designing the core elastic deformation mechanism. The series-parallel hybrid type of elastic mechanism usually has higher flexibility potential than the pure parallel configuration [14], where the 'rotary net' type of Fan *et al.* [15] and the 'earthworm' type of xx [13] are the representative ones.The increasing flexibility is ultimately limited to improving the accuracy of the probe. Based on the existing design of the probe, Cui *et al.* [16] arranged an electric field on the stylus ball to realize a new non-contact measurement mode, and they also proposed a photoelectric probe that does not rely on mechanical structures [17], which essentially solved the problem of friction. The usage scenarios of these types are limited and the usage methods are complicated.

In addition, friction or wear not only exists in macroscopic workpiece measurement, but also exists in molecular and atomic level measurement represented by atomic force microscope (AFM) [18]. AFM uses van der Waals force as the measurement feedback reference, and realizes multiple measurement modes. The tap mode combines the advantages of contact and non-contact measurement modes,

The associate editor coordinating the review of this manuscript and approving it for publication was Jingang Jiang.

which not only guarantees the measurement resolution, but also reduces or eliminates the lateral force or micro friction. National Physics Laboratory (NPL) also uses van der Waals force as a benchmark to propose a vibration measurement probe [14], [19], which uses high-frequency response and active strain feedback to achieve a real-time non-contact measurement mode. The above measurement modes generally vibrate at a resonance frequency, which is suitable in a nano-scale environment. For most probes used for measuring machined parts, the continuous vibration at the resonance frequency will inevitably accelerate the collision and wear on the stylus ball due to the contact force that is hundreds of times higher than that of AFM. Therefore, how to cleverly use the advantages of the vibration mode and avoid its shortcomings is very valuable for improving the performance of the probe.

We have done some work on the improvement of probe flexibility [20] and the mathematical elimination of friction force [9] before, and realize that friction force is difficult to be eliminated fundamentally in contact measurement. And if the friction force that changes according to the surface topography can be transformed into a constant friction force, then the measurement error caused by the friction can be eliminated as a constant in the results. Vibration mode with force feedback is a way to realize this idea, which includes the selection of vibration mode and the application of feedback. However, it is difficult to directly apply the resonance modes of hundreds of hertz to the existing passive probes, meaning the exploration of new vibration modes is more important.

Based on the body of a three-dimensional flexible probe [9], this paper explores a measurement mode for low-frequency vibration driven by piezoelectric actuators (PZT). The dynamic time-domain response function of the probe system is constructed based on the transfer function of the system and the triangular wave signals at different drive frequencies. The characteristics of the system response of the probe under various PZT drive frequencies are analyzed, and the advantages of low-frequency drive are summarized. Further, the nonlinear waveform of the triangular wave driven by the PZT low frequency, as well as the influence of nonlinearity on the scanning deviation is analyzed. Then, the method of nonlinear suppression based on non-uniform B-spline [21] and particle swarm optimization algorithm (PSO) [22] is proposed to realize the high-quality nonlinear suppression of the triangular wave and avoid the deviation of the shape detection during rapid scanning. Finally, the vibration measurement experiment of the probe is carried out to reveal the measurement characteristics of low-frequency mode as well as measurement capability compared with commercial sensors.

II. DESIGN AND VIBRATION ANALYSIS OF FLEXIBLE PROBE SYSTEM

A. PZT DRIVEN PROBE SYSTEM

The probe system uses a three-dimensional (3D) flexible probe containing an elastic deformation mechanism and a stylus as the mechanical body. During the measurement, the stylus of the probe is in contact with the measured surface, causing the elastic mechanism and the stylus to produce corresponding deflection under the generation and transmission of contact force. The deflection of the stylus is along the direction of the contact force, while the deformation of the elastic mechanism is along the z-direction, as shown in Fig.1(a). A simple PZT driven probe is formed by rigidly connecting the sheet-type PZT with the surface of the cantilever through epoxy resin, as shown in Fig. 1(b). The PZT driven by a specific voltage waveform can drive the cantilever to produce a controllable, repetitive and precise reciprocating movement along the z-direction, and the vibration properties of the cantilever are determined and unique. The real-time movement of the cantilever is monitored by the capacitive sensor. The time-varying force or displacement in the measurement will change the signal waveform of the system response in a non-interference state, where the changes of the signal magnitude and waveform are the key to obtaining high-precision measurement results.

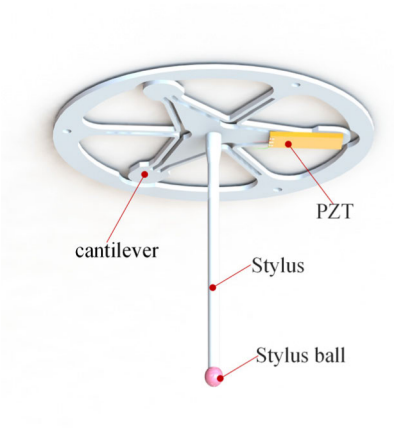

FIGURE 1. Structure of PZT driven probe system.

B. DISTURBANCE AND RESPONSE ANALYSIS OF THE PROBE SYSTEM

The PZT driven probe has a high flexibility, which limits the dynamic characteristics of the system [23], and determines the system response characteristics under different drive frequencies, which can be revealed by a dynamic time-domain response function.

The construction of the transfer function of the probe vibration system is shown in Equation (1). The deflection $f(t)$ under PZT drive is equivalent to the force $F(t)$ acting on the end of the cantilever, that is $F(t) = f(t)k$, where k is the linear stiffness corresponding to the cantilever displacement.

$$m\ddot{s} + c\dot{s} + ks = f(t)k \tag{1}$$

where m is the equivalent mass of the cantilever, c is the viscous damping coefficient of the probe system. Thus, the transfer function can be as follows.

$$G_s = \frac{k}{ms^2 + cs + k} \tag{2}$$

The PZT driven probe uses a triangular wave as the drive signal, which is superimposed by a series of sine waves of different frequencies and amplitudes. Equation (3) uses Fourier series to express the triangular wave with continuous periods.

$$f(t) = \frac{A}{2} + \sum_{i=1,3,5,\cdots} \frac{4A}{(i\pi)^2} \cos(iw_0 t), \quad w_0 = \frac{2\pi}{T} \tag{3}$$

model is

Where A is the amplitude, i is the i-th harmonic component, w_0 and T are the frequency and period of continuous triangular wave, respectively. The frequency domain expression of the triangular wave after Laplace transform is as follows.

$$L[f(t)] = \frac{A}{2s} + \sum_{i=1,3,5,\cdots} \frac{4As}{(i\pi)^2(i^2w^2 + s^2)}$$

The frequency-domain response of the probe system driven by a triangular wave at any frequency is thus as follows.

$$X_o = G_s L[f(t)]$$

The dynamic time-domain response function is further obtained by the inverse Laplace transform, as shown in Equation (4).

$$x(t) = Q_1 + 2Ak \sum_{i=1,3,5,\cdots} (Q_2 + Q_3) \tag{4}$$

where (Q_1)–(Q_3), as shown at the bottom of the page.

Q_1 characterizes the basic properties of the probe system, and has nothing to do with the drive frequency and system resonance. Q_3 represents the transient response components of the system related to the PZT drive state. Q_2 shows the superposition of various harmonic components in the system response. It can be seen that with the increase of the drive frequency, the dynamic coefficients related to w_0 show a nonlinear and sharp change. The i-th harmonic component in a series of sinusoidal harmonic components of the triangle wave first resonates, thus causing the i-th sinusoidal oscillation component to appear in the triangle wave of the system response. As the PZT drive frequency becomes larger, the i-2, i-4, . . . th order harmonic components resonate one after another, finally making the response waveform a standard sine wave.

III. DYNAMIC TEST AND ANALYSIS OF PZT DRIVEN PROBE

In order to study the response characteristics of probes at different PZT driven frequencies, an experimental test platform is built, including two parts: dynamic identification of the probe system and PZT frequency-driven experiment. The identification experiment is mainly to obtain the natural frequency and damping of the PZT driven probe, wihle the latter experiment is to select different drive frequencies from low too high to analyze the system response characteristics, so as to select the appropriate drive frequency for the probe. The experimental platform is shown in Fig. 2, including the probe, 3D pose adjustment device (Thorlabs, MBT616), PZT controller (Thorlabs, MDT693A), signal generator (Tektronix AFG3052C), linear guide system (Newport, IMS400BPP) and host computer, etc.

The probe is placed on one side of the guide rail, and the mirror surface on the posture adjustment device is facing the probe ball (Fig. 2(b)). The thin-film PZT (brand: Thorlabs, size: PB4VB2W) is mounted on a cantilever with epoxy resin as shown in Fig. 2(c). One end near the geometric center is a fixed end, and the other end is bent under voltage drive, which drives the cantilever to produce a micro displacement along the z-axis. The PZT controller amplifies the voltage of 0-5 V output by the signal generator to a maximum of 0-150 V.

A. DYNAMIC IDENTIFICATION OF THE PROBE

The experiment uses the free vibration-attenuation curve to obtain the first-order natural frequency and damping ratio of the probe system. The stylus ball and the mirror surface (Thorlabs, BBSQ2-E02) of the pose device are in pre-tightened contact, and the linear guide is set to a running speed of 60 mm/s to make relative movement between the stylus ball and the mirror surface. At the moment of separation from each other, the probe system will produce a free vibration-attenuation curve as shown in Fig. 3(a). The first-order natural frequency can be obtained by Fourier transform (Fig. 3(b)), and the damping ratio can be obtained according to the fitting curve of the outer envelope. The first-order natural frequency of the probe system is 140.7 Hz, and the damping ratio is 0.011.

$$Q_1 = \frac{A}{2} - \frac{Ae^{-ct/2m}}{2}\left[\cosh\left(\frac{t\sqrt{c^2-4km}}{2m}\right) + \frac{c\sinh\left(\frac{t\sqrt{c^2-4km}}{2m}\right)}{\sqrt{c^2-4km}}\right],$$

$$Q_2 = \frac{k\cos(iw_0t) - i^2mw_0^2\cos(iw_0t) + icw_0\sin(iw_0t)}{5i^2((icw_0)^2 + (i^2mw_0^2)^2 - 2kmi^2w_0^2 + k^2)},$$

$$Q_3 = \frac{(i^2mw_0^2 + k)e^{-ct/2m}\left(\cosh\left(\frac{t\sqrt{c^2-4km}}{2m}\right) + \frac{2c\sinh\left(\frac{t\sqrt{c^2-4km}}{2m}\right)(k-i^2mw_0^2)}{(-2i^2mw_0^2+2k)\sqrt{c^2-4km}}\right)}{5i^2((icw_0)^2 + (i^2mw_0^2)^2 - 2kmi^2w_0^2 + k^2)}$$

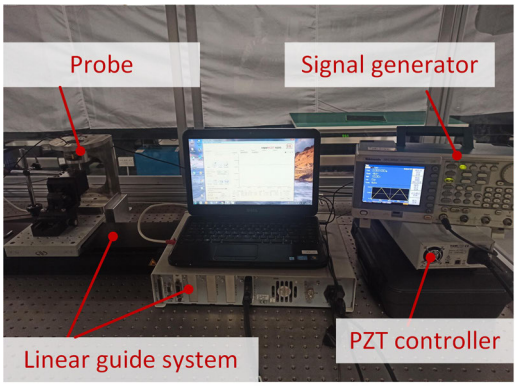

(a)

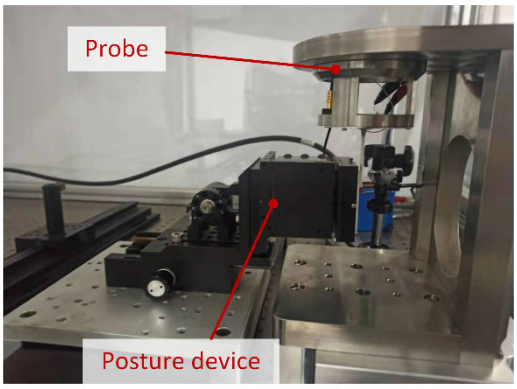

(b)

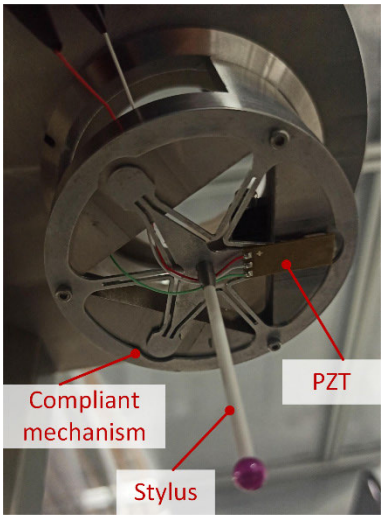

(c)

FIGURE 2. Experimental platform of PZT-driven probe, (a) all the equipment (b) the relative position of the probe and the pose device (c) the view of the probe.

B. PZT FREQUENCY-DRIVEN EXPERIMENT

In this experiment, a series of frequencies from low frequency to resonant frequency are selected as the drive frequency of PZT. The single-period waveform of the probe system driven by triangular waves of different frequencies is shown in Fig. 4. It can be seen that, the triangular waveform at 4 Hz is relatively standard, while there is a more obvious

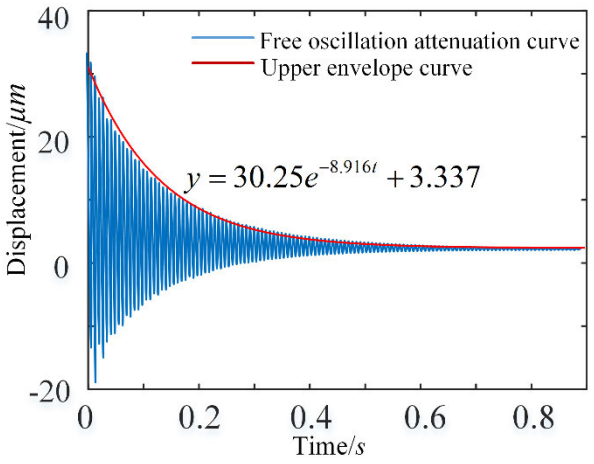

(a)

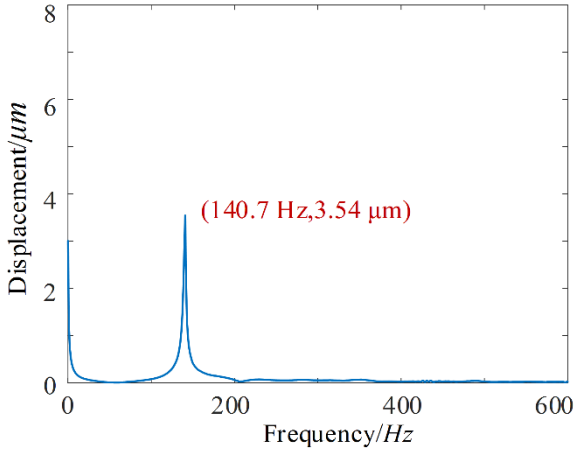

(b)

FIGURE 3. Dynamic properties of the probe system (a) free vibration-attenuation curve (b) First-order natural frequency.

harmonic interference component at 10 Hz. And the harmonic interference becomes more and more serious as the drive frequency continues to increase. At 80 Hz, the transition from a triangular wave to a sine wave is basically completed, and at the resonance frequency of 141 Hz, the triangular wave is completely transformed into a standard sine wave. In addition, the amplitude of the single-cycle waveform shows a nonlinear increase as the drive frequency increases. Compared with the 3.96 μm amplitude at 4 Hz, the amplitude at 20 Hz is amplified nearly 6 times to 22.62 μm. This phenomenon is consistent with the theoretical analysis in section *II. B*.

Analyzed from the measurement quality, only the low-frequency triangular wave without resonance influence and the sine wave at the resonance frequency are suitable as measurement benchmarks to perceive real-time stimulation of external force or displacement. The advantages of resonant frequency drive are large amplitude and dense signal, but it also brings accelerated fatigue of the deforming structure of the probe, and the touch force in the measurement of workpieces is hundreds of times higher than that

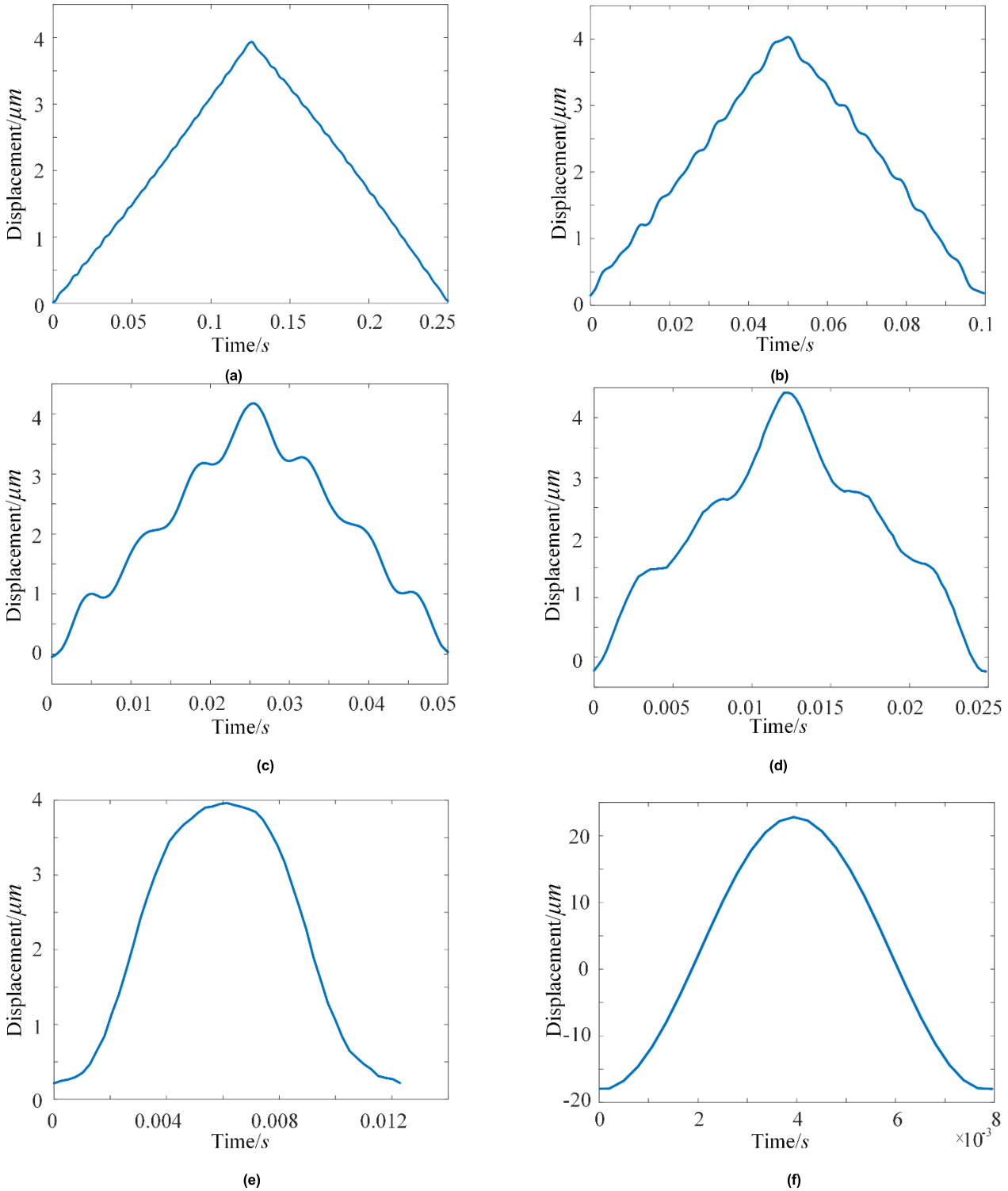

FIGURE 4. The gradual change of the response waveform under different PZT-driven frequency (drive voltage, 60V) (a) 4 Hz (b) 10 Hz (c) 20 Hz (d) 40 Hz (e) 80 Hz (f) 141 Hz.

in the AFM scene, which can easily lead to abrasion of the probe ball and surface. While the adjustable linear waveform under low drive frequency has high displacement sensitivity while avoiding the destructiveness caused by large vibrations of hundreds of Hz. The matching of driving frequency and scanning speed makes the probe have sufficient spatial resolution and accuracy [5]. More importantly, the selectable range of low drive frequency will be expanded through miniaturization and structural optimization of the probe.

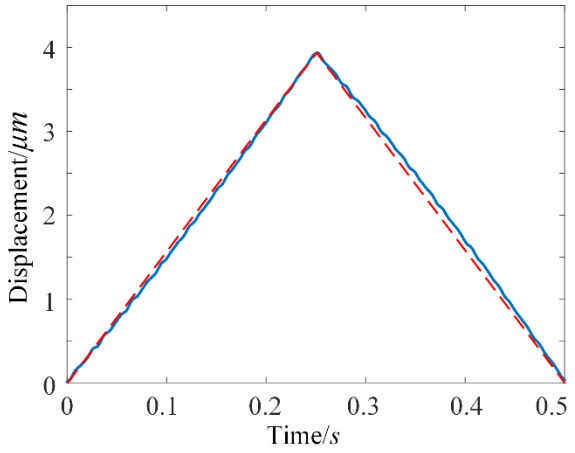

FIGURE 5. Non-linear waveform driven by 2 Hz triangle wave.

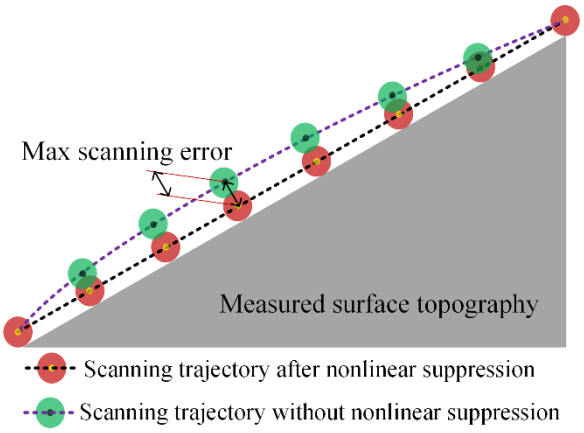

FIGURE 6. The deviation of the scan trajectory before and after nonlinear suppression.

IV. NONLINEAR SUPPRESSION OF PZT LOW-FREQUENCY DRIVE BASED ON PSO

A. ANALYSIS OF PZT HYSTERESIS MODEL

The inherent hysteresis of PZT poses a challenge to the maintenance of the linear waveform of the triangular wave in the response of the probe system. As shown in Fig. 5, the triangular wave in the system response shows obvious nonlinearity under the drive frequency of 2 Hz, of which the influence on the measurement results is shown in Fig. 6. In the half-cycle scanning of the triangular wave, the nonlinear problem will cause the probe ball to separate from the measured surface, resulting in a significant measurement deviation. For the surface with complex morphology, this effect will be more obvious. Therefore, in order to ensure the high quality of the response waveform as a measurement reference, nonlinear hysteresis should be suppressed.

The experiment uses low frequency of 1-5 Hz as the preselected drive frequency to construct the hysteresis model of the probe system, and explores the response characteristics of the probe at five different frequencies, as shown in Fig. 7. It is found that the hysteresis characteristics of the thin-film PZT have considerably affected the reference accuracy

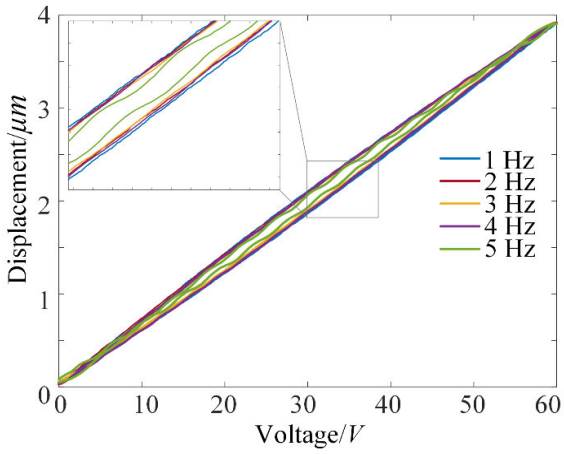

FIGURE 7. Hysteresis models under low frequency drive.

of the probe. The difference of the hysteresis model under different drive frequencies is not very significant, but the hysteresis model produces a larger harmonic vibration at 5 Hz with the fluctuation amplitude of about 0.1 μm. To avoid this phenomenon, the appropriate low frequency should be determined as 2, 3, 4 Hz.

In order to study the relationship between the hysteresis nonlinearity of the probe system and the drive voltage, the hysteresis model distribution of the probe system in the range of 30-150V under the drive frequency of 2, 4 Hz is analyzed. As shown in Fig. 8, the nonlinearity of the waveform becomes more obvious as the driven voltage rises, and it is especially reflected in the middle and low voltage range. In addition, it can be seen that there is also micro vibrations at 4 Hz, which has little effect on accuracy due to the small amplitude.

B. NON-LINEAR SUPPRESSION METHODS AND EXPERIMENTS

To obtain high-quality detection signal, the hysteresis nonlinearity should be suppressed. BP neural network, non-uniform B-spline and PSO algorithm with linear weight reduction are used to correct the nonlinear waveform. The standard triangle wave is used as the ideal output, and the corresponding actual input voltage curve is obtained in turn. First, the BP neural network is used to fit the nonlinear mapping relationship between actual input voltage and actual output displacement at different drive frequencies, and the nonlinear neural network model of the PZT driven probe at specific frequency is obtained. Next, a non-uniform B-spline curve is used to adjust the rising and falling edges of the triangle wave with 21 control points, as shown in Fig. 9. Then, PSO algorithm is used to generate voltage random numbers, and the control point of the B-spline is adjusted and optimized one by one within the range of random numbers. The criterion for the optimization of the control points is that the difference between the adjusted output value of the B-spline and the mapping under the nonlinear neural network model

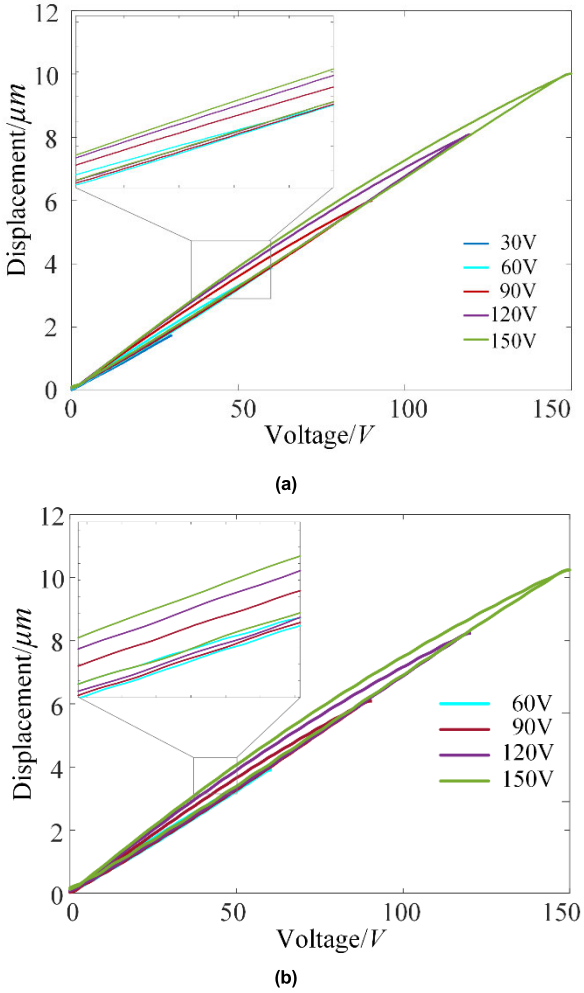

FIGURE 8. Hysteresis model under different voltage (a) drive frequency of 2 Hz and (b) 4 Hz.

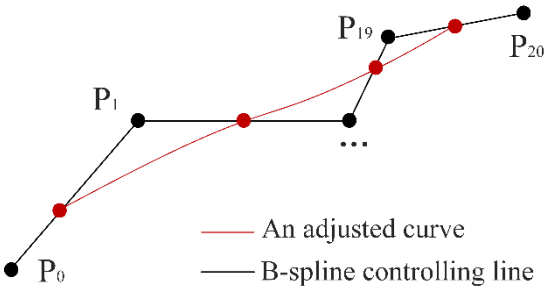

FIGURE 9. B-spline control line and points.

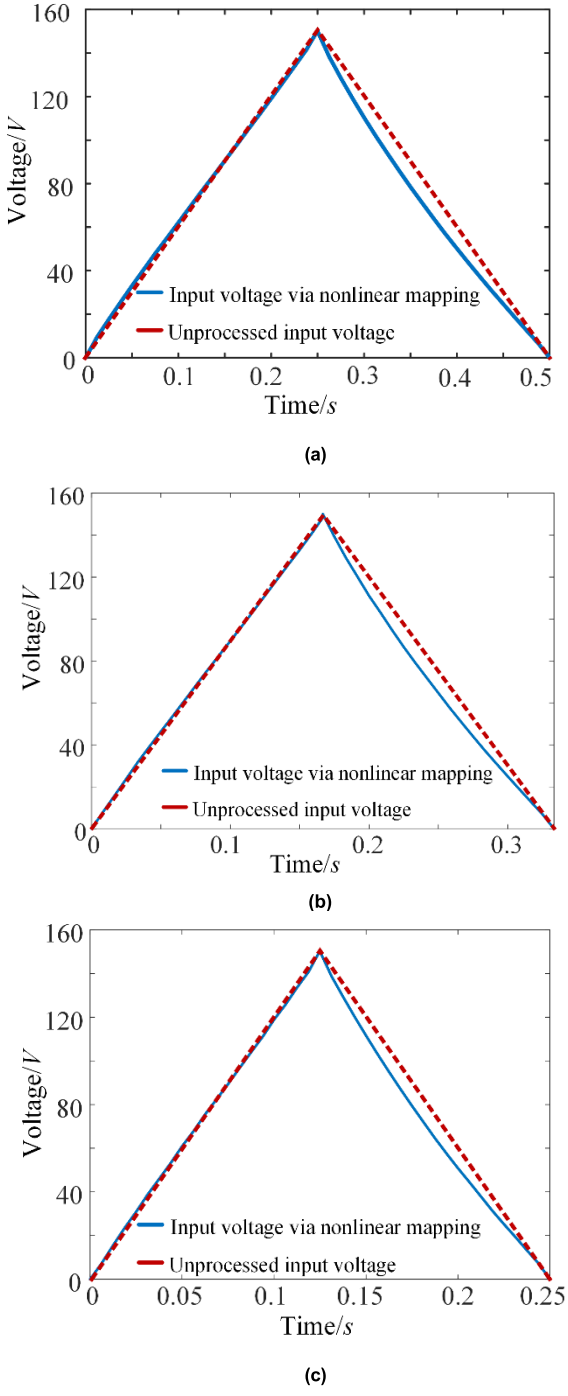

FIGURE 10. Actual drive voltage after nonlinear suppression processing.

is less than the set convergence value. Otherwise, it will automatically reset the weight of PSO algorithm, regenerate random numbers and repeat the optimization, mapping, and comparison process, until finally find the actual input voltage curve that meets the conditions.

Considering that the non-linearity under the maximum voltage of 150 V is the most significant, the experiment studies the suppression of the response non-linearity at three frequencies of 2, 3, and 4 Hz. According to the peak displacement obtained under the voltage of 150V in the previous experiment, the ideal output linear expression is established. After that, the mapping calculation of the actual input voltage curve is completed according to the above optimization and solution process.

The actual input voltage constructed by the above method is shown in Fig. 10. It can be seen that there is a significant difference between the input voltage curve without any processing and through the nonlinear mapping calculation. The

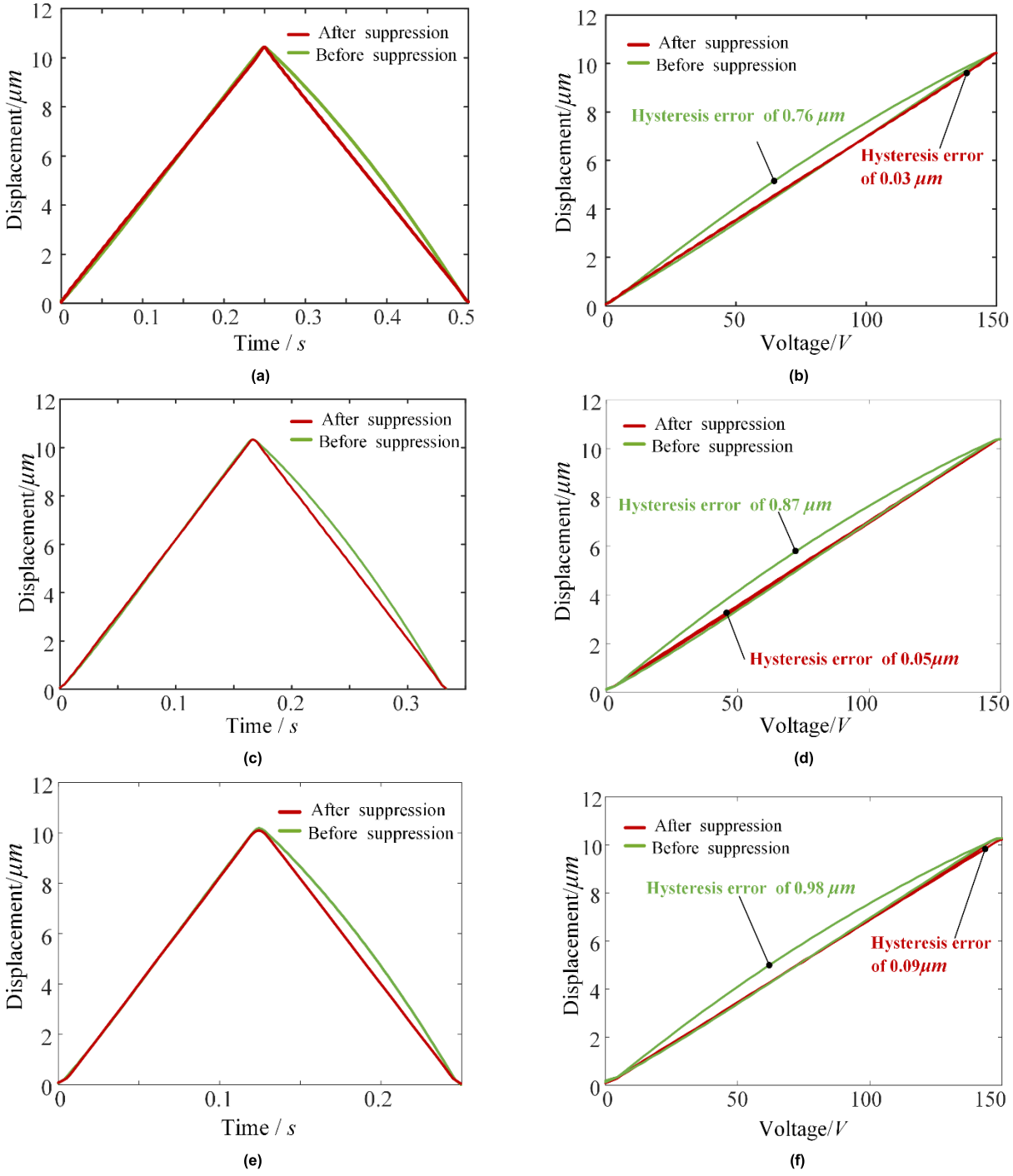

FIGURE 11. Non-linear suppression effect under low frequency drive (a) triangular waveform at 2 Hz and hysteresis loop (b) at 2 Hz, (c) triangular waveform at 3 Hz and hysteresis loop (d) at 3 Hz, (e) triangular waveform at 4 Hz and hysteresis loop (f) at 4 Hz.

rising edge changes slightly after being mapped, while the falling edge arc changes significantly. From the characteristic analysis of the actual voltage curve, the higher the drive frequency, the smaller the arc of the falling edge, indicating that the difference between the general voltage and the correction voltage is smaller.

The actual voltage curve obtained by nonlinear suppression is then applied to drive the flexible probe. The single-period triangular wave in the system response after nonlinear correction is presented in Fig. 11 (a) (c) (e), showing the linearity under the three drive frequencies is significantly improved. Table 1 shows the change of the correlation coefficient R2 of

TABLE 1. Comparison of correlation coefficient R^2 before and after nonlinear suppression.

		2 Hz	3 Hz	4 Hz
Before suppression	Rising edge	0.999814	0.999691	0.999680
	Falling edge	0.995544	0.994027	0.994003
After suppression	Rising edge	0.999892	0.999860	0.999771
	Falling edge	0.999904	0.999826	0.999799

the fitted curve before and after optimization. It can be seen that the linearity of the rising edge of PZT itself is much better than that of the falling edge. After nonlinear suppression, the linearity of the falling edge of the PZT driven system is greatly improved.

On the other hand, due to the difference in the nonlinearity of the triangular wave at different drive frequency, the maximum hysteresis error of the hysteresis loop is also different. Fig. 11 (b) (d) (f) shows that, the proposed suppression method has greatly reduced the hysteresis error, guaranteed the linear movement of the stylus ball during the scanning, and avoided the surface separation that may be caused.

V. MEASUREMENT EXPERIMENT OF PZT DRIVEN PROBE

A. EXPERIMENTAL ANALYSIS OF MEASUREMENT MODE

In order to explore the sensing mode of the PZT-driven probe in the vibration measurement, a single-point reciprocating motion experiment is designed, and the measurement principle of the probe in the vibration mode is analyzed. During the probe start-up phase, the transient waveform superimposed on the triangular wave will appear in the response signal first, and then gradually disappear, as shown in Fig. 12. It can be seen that the greater the drive frequency, the more significant the transient waveform, indicating that the transient amplitude is directly related to the drive frequency w_0, which has been already stated by Equation (3).

To obtain the measurement principle in the vibration mode, this experiment uses the pose adjustment device in Fig. 2(b) to continuously and randomly adjust the relative position between the smooth mirror and the vibrating stylus ball, and obtain the measurement data shown in Fig. 13. It can be seen that, there is a significant "blank" area in the signal during the measurement period, indicating that the external displacement has applied linear modulation to the waveform. In addition to the obvious change in peak value, the linear waveform of the triangular wave during the free vibration period is very standard (Fig. 13(b)), while the waveform during the measurement period has a nonlinear distortion (Fig. 13(c)). In a period of the drive frequency of 2 Hz, the stylus ball moving along the rising or falling edge of the triangle wave maintains continuous contact with the external displacement trajectory, which in turn causes the modulated deformation of the waveform as described in Fig. 6.

By constructing the data tables before and after the measurement, the difference between the two, that is, the actual measurement curve is obtained, as shown in Fig. 14. The outer envelope of the measurement area is used to express

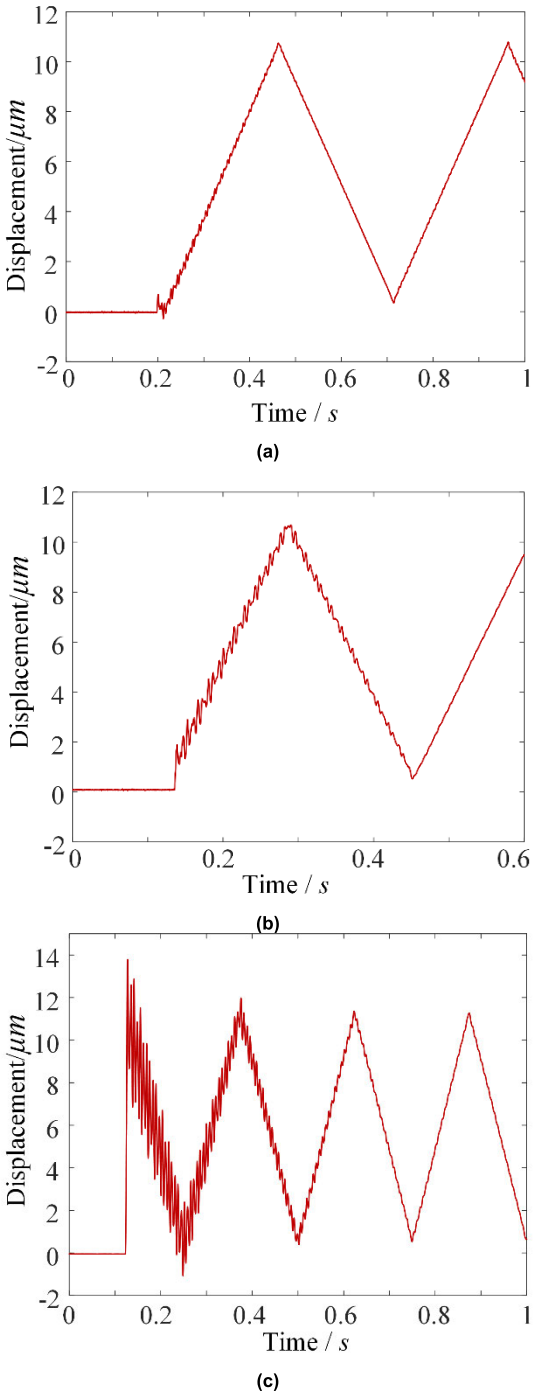

FIGURE 12. Start-up waveform at different frequencies (a) 2 Hz (b) 3 Hz (c) 4 Hz.

the contour of the continuous measured displacement. The higher the drive frequency, the closer the outer envelope is to the real displacement curve.

B. COMPARATIVE ANALYSIS OF EXPERIMENTAL RESULTS

The greater the drive frequency, the more data points collected per unit time, and the more complete the external contour. The experiment under the frequency of 4 Hz continues,

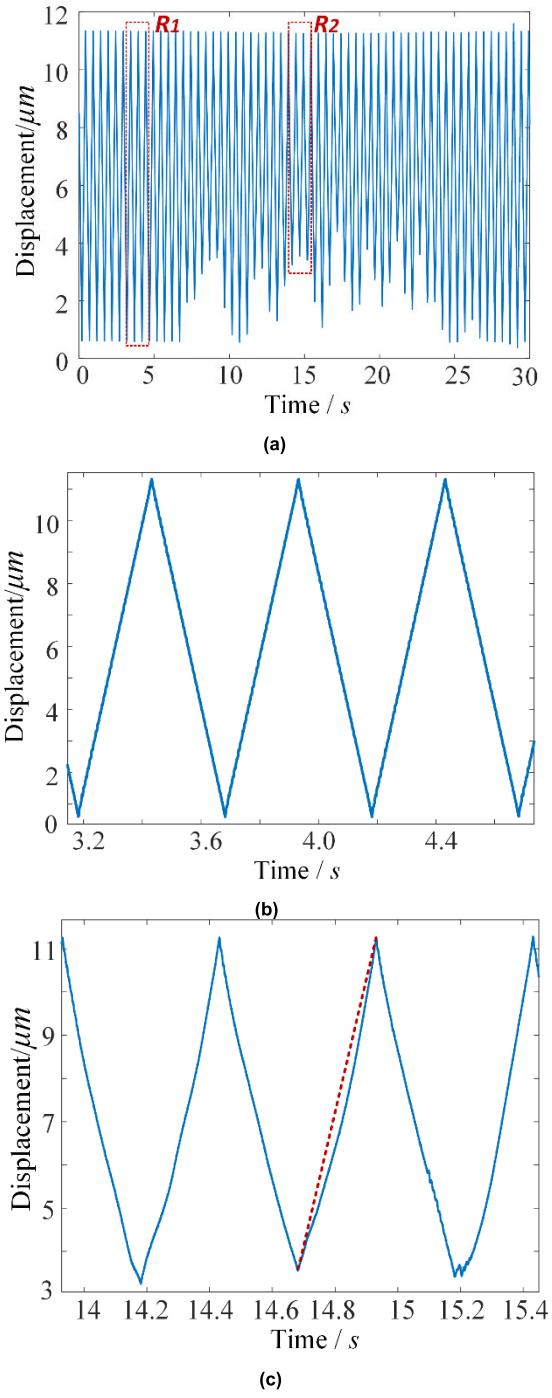

FIGURE 13. Analysis of measurement waveforms.

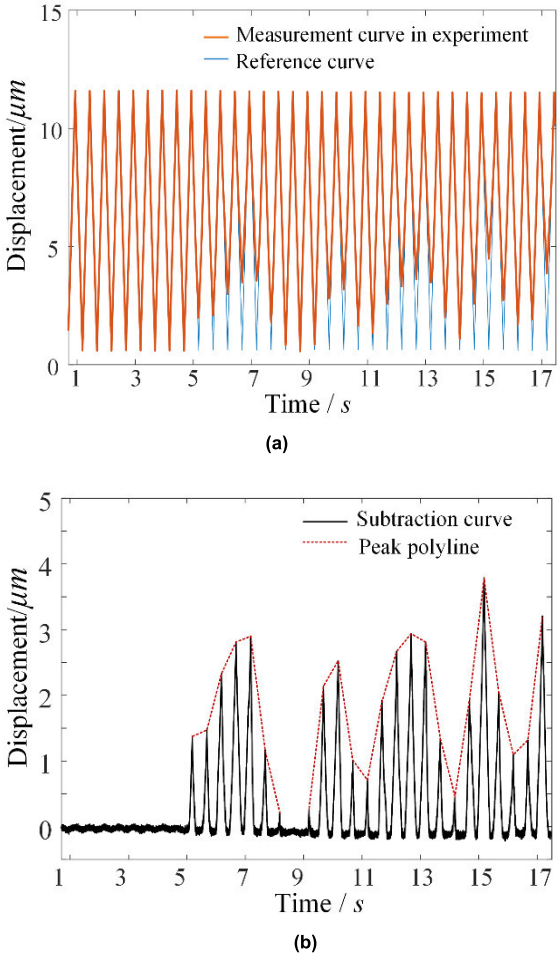

FIGURE 14. Analysis of measurement results (a) Comparison of measurement curves (b) Difference curve between the real and reference data.

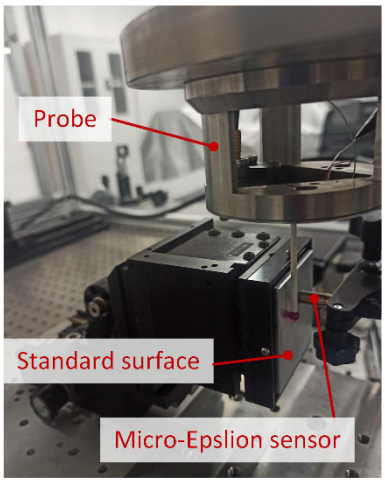

FIGURE 15. Measurement experiment for random normal displacement.

still taking random normal displacement as the detection object, and using the third-party commercial sensor-German Micro-Epsilon sensor (CS02) as the reference measurement instrument, as shown in Fig. 15. The M-E sensor has high dynamic resolution of up to 40 nm. After the PZT starts to drive, the posture device is adjusted to make the standard surface and the stylus ball have a micro contact. Then, the micron-level feed of the precision adjustment axis on the pose device is manually operated to generate random relative movement between the stylus ball and the surface in the normal direction.

As shown in Fig. 16, the measurement signal under the drive frequency of 4 Hz has richer details and higher spatial

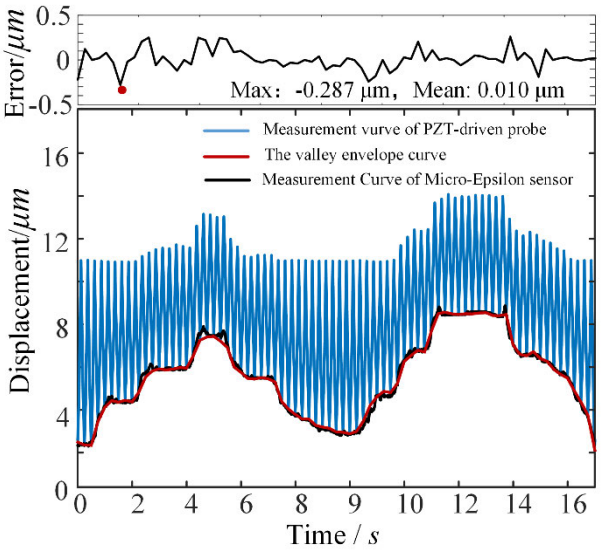

FIGURE 16. **Measurement analysis at the drive frequency of 4 Hz.**

resolution than that of 2 Hz. More importantly, the normal displacement exceeds the amplitude of the free oscillation of the probe, thus delineating a wide range of blank areas, of which the valley envelope reflects the movement trajectory of the measured surface. Besides, the measurement curve detected by Micro-Epsilon sensor is compared with the result of the PZT-driven probe, and the error graph shows the maximum error is -0.287 μm and the average error is 0.010 μm. The reason for the maximum error is that, the normal displacement under manual adjustment easily leads to shock waveforms as the displacement changes suddenly. At this time, the stylus ball is being in the moving track of the rising or falling edge of the triangle wave, and the waveform of the shock wave is coupled with the rising or falling edge and is submerged. For example, the measurement curve of Micro-Epsilon sensor during 4-6 s has two obvious spikes, which are larger than the error in the error graph.

VI. CONCLUSION

Through sufficient theoretical and experimental research, the system response characteristics of the probe under various drive frequencies are fully analyzed. In the resonance mode, the hitting frequency of hundreds of Hz on the measured surface greatly increases the risk of collision and wear of the stylus ball, while the touch force of the probe is hundreds of times that of AFM. In comparison, although the low-frequency drive mode has led to a significant reduction in the number of measurement points per unit time and the discretization of the contour, the characteristic of relying on the natural frequency of the mechanical body makes this mode has sufficient potential for application. This experiment uses a flexible mechanism with a natural frequency of only 141 Hz. For every 100 Hz increase in the natural frequency, the upper limit of the drive frequency can be increased by 3-4 Hz. Besides, the proposed PZT nonlinear suppression method greatly improves the detection accuracy of the senor and ensures the high quality of the measurement signal.

Moreover, the low-frequency drive mode can achieve the effect of dense-point measurement by matching the appropriate scanning speed [4], [24], but it is impossible to eliminate the error effect of time-varying friction without feedback. Therefore, it is intended to increase the force feedback module on this basis to keep the contact force as well as friction force between the stylus ball and measured surface constant, so that the value of the low-frequency drive mode can be further expanded.

REFERENCES

[1] J. Guo and M. Martínez-García, "Key technologies towards smart manufacturing based on swarm intelligence and edge computing," *Comput. Electr. Eng.*, vol. 92, Jun. 2021, Art. no. 107119.

[2] H. Hinduja, S. Kekkar, and S. Chourasia, "Industry 4.0: Digital twin and its industrial applications," *RIET-IJSET Int. J. Sci. Eng. Technol.*, vol. 8, no. 4, pp. 1–7, Aug. 2020.

[3] T. H.-J. Uhlemann, C. Lehmann, and R. Steinhilper, "The digital twin: Realizing the cyber-physical production system for industry 4.0," *Procedia CIRP*, vol. 61, pp. 335–340, Jan. 2017.

[4] G. Krajewski and A. Woźniak, "Simple master artefact for CMM dynamic error identification," *Precis. Eng.*, vol. 38, no. 1, pp. 64–70, Jan. 2014.

[5] A. Wozniak, G. Krajewski, and M. Byszewski, "A new method for examining the dynamic performance of coordinate measuring machines," *Measurement*, vol. 134, pp. 814–819, Feb. 2019.

[6] B. Muralikrishnan, J. A. Stone, and J. R. Stoup, "Fiber deflection probe for small hole metrology," *Precis. Eng.*, vol. 30, no. 2, pp. 154–164, Apr. 2006.

[7] A. Nicolet and A. F. K. Meli, "Study of sapphire probe tip wear when scanning on different materials," *Meas. Sci. Technol.*, vol. 23, no. 9, pp. 1425–1437, Sep. 2012.

[8] P. Kinnell and R. Habeb, "The unpredictable errors of micro tactile metrology—Factors affecting stylus tip contamination," *Meas. Sci. Rev.*, vol. 13, no. 6, pp. 305–310, Dec. 2013.

[9] W. Zheng, Z. Liu, and J. Guo, "A friction-coupled measurement model of a 3D scanning probe with unequal stiffness," *Meas. Sci. Technol.*, vol. 32, no. 1, Jan. 2021, Art. no. 015106.

[10] P. H. Pereira and R. J. Hocken, "Characterization and compensation of dynamic errors of a scanning coordinate measuring machine," *Precis. Eng.*, vol. 31, no. 1, pp. 22–32, Jan. 2007.

[11] R.-J. Li, K.-C. Fan, Q.-X. Huang, H. Zhou, E.-M. Gong, and M. Xiang, "A long-stroke 3D contact scanning probe for micro/nano coordinate measuring machine," *Precis. Eng.*, vol. 43, pp. 220–229, Jan. 2016.

[12] T. Liebrich and W. Knapp, "Improvements and experimental validation of a 3D-probing system for micro-components," *CIRP Ann.*, vol. 61, no. 1, pp. 475–478, 2012.

[13] M. He, R. Liu, Y. Li, H. Wang, X. Lu, G. Ding, J. Wu, T. Zhang, and X. Zhao, "Tactile probing system based on micro-fabricated capacitive sensor," *Sens. Actuators A, Phys.*, vol. 194, pp. 128–134, May 2013.

[14] J. D. Claverley and R. K. Leach, "Development of a three-dimensional vibrating tactile probe for miniature CMMs," *Precis. Eng.*, vol. 37, no. 2, pp. 491–499, Apr. 2013.

[15] P. Xu, R. J. Li, X. W. Jin, P. Y. Wang, L. J. Chen, and K. C. Fan, "A new micro/nano-touch-trigger probe using an optoelectronic sensor with a wedge prism," *Rev. Sci. Instrum.*, vol. 91, no. 7, Jul. 2020, Art. no. 076103.

[16] X. Bian, J. Cui, Y. Lu, and J. Tan, "Ultraprecision diameter measurement of small holes with large depth-to-diameter ratios based on spherical scattering electrical-field probing," *Appl. Sci.*, vol. 9, no. 2, p. 242, Jan. 2019.

[17] K. Feng, J. Cui, X. Sun, H. Dang, T. Shi, Y. Niu, and J. Tan, "A tapered fourcores phase-shift FBG probe for three-dimensional micro-scale measurement," *IEEE Photon. Technol. Lett.*, vol. 30, no. 20, pp. 1799–1802, Oct. 15, 2018.

[18] P. Eaton and P. West, *Atomic Force Microscopy*. London, U.K.: Oxford Univ. Press, 2010.

[19] J. D. Claverley and R. K. Leach, "A vibrating micro-scale CMM probe for measuring high aspect ratio structures," *Microsyst. Technol.*, vol. 16, nos. 8–9, pp. 1507–1512, Aug. 2010.

[20] W. Zheng, Z. Liu, X. Li, and J. Guo, "An optimized 3D displacement probe using sensitivity-compliance joint model," *Rev. Sci. Instrum.*, vol. 90, no. 10, Oct. 2019, Art. no. 105003.
[21] T. T. N. Nguyen, S. Kurtenbach, M. Hüsing, and B. Corves, "A general framework for motion design of the follower in cam mechanisms by using non-uniform rational B-spline," *Mechanism Mach. Theory*, vol. 137, pp. 374–385, Jul. 2019.
[22] J. Kennedy, "Particle swarm optimization," in *Proc. IEEE Int. Conf. Neural Netw.*, Perth, WA, Australia, vol. 4, no. 8, Dec. 2011, pp. 1942–1948.
[23] S. Devasia, E. Eleftheriou, and S. O. R. Moheimani, "A survey of control issues in nanopositioning," *IEEE Trans. Control Syst. Technol.*, vol. 15, no. 5, pp. 802–823, Sep. 2007.
[24] W. Jinwen and C. Yanling, "The geometric dynamic errors of CMMs in fast scanning-probing," *Measurement*, vol. 44, no. 3, pp. 511–517, Mar. 2011.

WEIKANG ZHENG received the B.E. degree in mechanical engineering and automation from the Ocean University of China, Qingdao, China, in 2015. He is currently pursuing the Ph.D. degree in mechanical engineering with Xi'an Jiaotong University. His research interests include the design, modeling, and control of flexible sensors, and related technology of micro/nano measurement.

KAI TIAN received the B.E. degree in mechanical engineering from Northeastern University, Shenyang, China, in 2018. He is currently pursuing the Ph.D. degree in mechanical engineering with Xi'an Jiaotong University. His research interests include the control of external cavity diode laser and frequency scanning interferometery for absolute distance measurement.

JUNKANG GUO (Member, IEEE) received the B.S. and M.S. degrees in mechanical engineering from Central South University, and the Ph.D. degree in mechanical engineering from Xi'an Jiaotong University, Xi'an, China. He is currently an Assistant Researcher of mechanical engineering with Xi'an Jiaotong University. His research interests include data driven performance analysis and assembly process optimization technology for mechanical systems and digital twin technology for dimensional engineering and its application.

ZHIGANG LIU (Member, IEEE) received the B.E. degree from the Huazhong University of Science and Technology, in 1993, the master's degree from the Xi'an University of Technology, in 1996, and the Ph.D. degree from Xi'an Jiaotong University, China, in 2000. He is currently a Professor with the School of Mechanical Engineering, Xi'an Jiaotong University. His research interests include large scale 3D measurement, frequency scanning interferometer for absolute distance measurement, external cavity diode laser, and nano-positioning.

JUN HONG (Member, IEEE) received the B.S. degree in mechanical engineering from the North University of China, Taiyuan, China, in 1989, and the M.S. and Ph.D degrees in mechanical engineering from Xi'an Jiaotong University, Xi'an, China, in 1994 and 2001, respectively. He is currently a Professor of mechanical engineering with Xi'an Jiaotong University. His research interests include assembly mechanism of complex precision machinery, multidisciplinary design optimization, computational mechanics, and knowledge-based engineering.